Prediction of Turbulent Flow Around a Square Cylinder With Rounded Corners

S. S. Dai[1]
Deep Water Engineering Research Center,
Harbin Engineering University,
Harbin 150001, China

B. A. Younis
Department of Civil and
Environmental Engineering,
University of California,
Davis, CA 95616

H. Y. Zhang
Deep Water Engineering Research Center,
Harbin Engineering University,
Harbin 150001, China

Predictions are reported of the two-dimensional turbulent flow around a square cylinder with rounded corners at high Reynolds numbers. The effects of rounded corners have proved difficult to predict with conventional turbulence closures, and hence, the adoption in this study of a two-equation closure that has been specifically adapted to account for the interactions between the organized mean-flow motions due to vortex shedding and the random motions due to turbulence. The computations were performed using OPENFOAM *and were validated against the data from flows past cylinders with sharp corners. For the case of rounded corners, only the modified turbulence closure succeeded in capturing the consequences of the delayed flow separation manifested mainly in the reduction of the magnitude of the lift and drag forces relative to the sharp-edged case. These and other results presented here argue in favor of the use of the computationally more efficient unsteady Reynolds-averaged Navier-Stokes approach to this important class of flows provided that the effects of vortex shedding are properly accounted for in the turbulence closure.*
[DOI: 10.1115/1.4035957]

Keywords: vortex shedding, rounded corners, modified k–ϵ, force coefficients, turbulence closures

1 Introduction

In the field of ocean engineering, floating structures are frequently exposed to currents and wind at high Reynolds number and are hence subjected to the hydro- and aero-dynamic loads associated with the turbulent fluid motion. An essential mechanism in the generation of these loads is the reversal in flow direction of the fluid in the wake of a structure leading to the establishment of a region of reduced pressure, and a net drag force leading to drift. Often, the separation is unsteady leading to the alternate shedding of vortices. Due to the action of vortex excitation, the phenomenon of resonance can occur with consequent undesirable effects. Thus, the accurate simulation of the flow and the resulting loads on structural elements of various cross-sectional shapes are important components in the design and operation of offshore installations.

The aim of our study is to contribute to the body of knowledge in this field. The focus is on the prediction of the high Reynolds-number flows around cylinders that are square in cross section but whose corners are rounded. The effects of rounding the corners turn out to be quite substantial and difficult to predict. This is because, unlike in the case of flow around a cylinder with sharp corners, the location of the separation point here is not fixed a priori and hence must be predicted by accurately capturing the balance of the forces of inertia, friction, and pressure. Bearman et al. [1] investigated the effects of corner radius on the hydrodynamic forces on cylindrical bluff bodies that were placed in steady and oscillatory flows. They found that the value of drag coefficient was quite sensitive to the effects of rounded corners when the incident flow was steady and to a greater extent in the case of an oscillatory flow. Kawai [2] investigated the effects of various corner modifications (such as corner cut, recession, and rounding) on the characteristics and patterns of flows past rounded square cylinders and concluded that, of the various modifications tested, the rounding of the cylinder corners offered the best option for enhancing the aerodynamic stability of the cylinder via reduction of the resulting unsteady forces. Tamura et al. [3] and Tamura and Miyagi [4] investigated numerically and experimentally the effects of corner modification on the aerodynamic forces on square cylinders and observed a decrease in the wake width as well as the mean and root-mean-square values of the lift and drag coefficients by about 10%. Similarly, Dalton and Zheng [5], in a numerical study of the uniform flow past square and diamond cylinders with and without corner modifications, reported that rounding the corners of the bluff bodies produced a noticeable decease in the calculated drag and lift coefficients. Miran and Sohn [6] numerically studied the influence of corner radius on flow past a square cylinder at the relatively low Reynolds number $Re = 500$. They found that the minimum values of the mean drag coefficient and the root mean square value of the lift coefficient occurred at a ratio of corner radius (R) to square side (D) of around 0.2. Jaiman et al. [7] numerically studied the effect of rounded corner on stationary and freely vibrating square cylinders at values of Re in the range100–200, and they too found that rounding of corners delays the primary separation and with that the forces on the cylinders. Carassale et al. [8] investigated the influence of corner shaping on the aerodynamic behavior of cylinders through wind tunnel tests for two different rounded-corner radii and for values of Reynolds number in the range 1.7×10^4 to 2.3×10^5. Their interest was directed largely to the investigation of the flow behavior as a function of the angle of incidence, and found that the effects of rounding the corners are to reduce the critical angle of incidence for which the flow reattaches on the lateral surfaces. Ajith Kumar et al. [9] also experimentally investigated the near wake flow field of transversely oscillating square section cylinder with different corner radii by using the particle image velocimetry (PIV) technique in a water channel. They found that increasing the corner radius suppresses the potential for unsteady instabilities of the cylinder. Hu et al. [10] obtained measurements in the near wake of square cylinders with different corner radii using PIV, laser Doppler anemometry (LDA), and hot-wire techniques. Among their findings was the observation that as the ratio of corner radius to side length increases from 0 to 0.5, the maximum vorticity of the shed vortices is reduced, while their shape changes from being approximately circular to being laterally stretched. Nidhul [11] studied the influence of corner geometry on flow characteristics for flow past two-dimensional square cylinder at $Re = 150$, and

[1]Corresponding author.
Contributed by the Ocean, Offshore, and Arctic Engineering Division of ASME for publication in the JOURNAL OF OFFSHORE MECHANICS AND ARCTIC ENGINEERING. Manuscript received June 30, 2016; final manuscript received January 18, 2017; published online April 11, 2017. Assoc. Editor: David R. Fuhrman.

reported on the pressure and wall shear stress distributions along the cylinder wall. Delany and Sorensen [12] investigated the variation of the low-speed drag coefficient of cylinders of various shapes with three different corner radii at different Reynolds number. They found that the drag coefficient decreased with increase of the corner radius ratio.

It is clear from the above that the effects of corner modification on the overall flow behavior, and especially very close to the cylinder, are quite substantial and manifest in the form of reduction in the mean and fluctuating forces relative to the sharp-corners case. It is also clear that the majority of the previous studies have been for flows at Reynolds number that are far below those that are encountered in practice. In this study, we focus on the more difficult case where the Reynolds number is high and the flow is fully turbulent, and investigate how best to represent the effects of turbulence in the case of square cylinders with rounded corners.

2 Computational Details

2.1 Governing Equations. We adopt the unsteady Reynolds-averaged approach to solve the Navier–Stokes equations (URANS) in which the equations governing the conservation of mass and momentum for an incompressible fluid can be written as follows:

$$\frac{\partial}{\partial x_j}(U_j) = 0 \tag{1}$$

$$\frac{\partial U_i}{\partial t} + U_j \frac{\partial U_i}{\partial x_j} = \frac{\partial}{\partial x_j}\left(\nu \frac{\partial U_i}{\partial x_j} - \overline{u_i u_j}\right) - \frac{1}{\rho}\frac{\partial p}{\partial x_i} \tag{2}$$

where U_i is the mean-velocity vector, u_i is the fluctuating velocity, p is the mean pressure, ν and ρ are, respectively, the kinematic viscosity and density. The turbulence correlations $\overline{u_i u_j}$ that appear in Eq. (2) are the unknown Reynolds stresses that need to be determined by the use of a turbulence closure.

The turbulence closure used in this paper is of the eddy-viscosity type, that is, very widely used in offshore engineering. It utilizes Boussinesq's linear stress–strain relationship to relate the unknown Reynolds stresses to the local mean rates of strain, thus

$$-\overline{u_i u_j} = \upsilon_i\left(\frac{\partial U_i}{\partial x_j} + \frac{\partial U_j}{\partial x_i}\right) - \frac{2}{3}\delta_{ij}k \tag{3}$$

where υ_t is the eddy viscosity, and k is the turbulence kinetic energy. The eddy viscosity is obtained by the k–ϵ two-equation model of turbulence chosen for this study via the relationship

$$\nu_t = C_\mu \frac{k^2}{\varepsilon} \tag{4}$$

In Eq. (4), C_μ is a coefficient determined by the reference to experimental data, and ε is the rate of dissipation of k due to viscous action. The quantities k and ε are obtained from the solution of their own transport equations. Those are given by

$$\frac{\partial k}{\partial t} + U_j \frac{\partial k}{\partial x_j} = \frac{\partial}{\partial x_j}\left(\left(\nu + \frac{\nu_t}{\sigma_k}\right)\frac{\partial k}{\partial x_j}\right) + P_k - \varepsilon \tag{5}$$

$$\frac{\partial \varepsilon}{\partial t} + U_j \frac{\partial \varepsilon}{\partial x_j} = \frac{\partial}{\partial x_j}\left(\left(\nu + \frac{\nu_t}{\sigma_\varepsilon}\right)\frac{\partial \varepsilon}{\partial x_j}\right) + C_{\varepsilon 1}\frac{\varepsilon}{k}P_k - C_{\varepsilon 2}\frac{\varepsilon^2}{k} \tag{6}$$

where σ_ε and σ_k are coefficients, and P_k is the rate of production of k

$$P_k = -\overline{u_i u_j}\frac{\partial U_i}{\partial x_j} \tag{7}$$

It is now well documented in the literature that the standard k–ϵ model fails badly in the prediction of flows dominated by vortex shedding. Specifically, it predicts a far weaker vortex shedding strength (as characterized, for example, by the root-mean-square values of the lift and drag coefficients) than is observed in measurements [13,14]. Younis and Przulj [15] have argued that the reason for this shortcoming lies in the fact that the standard model has been formulated by reference to data from stationary flows where a state of equilibrium is established between the rate of generation of turbulence by the interaction of the steady mean shear with the turbulent stresses, and the rate of dissipation of turbulence by the action of viscosity on the small-scale motions. However, when vortex shedding is present, an additional source of turbulence generation is introduced, arising from the oscillations of the mean flow field at a discrete frequency that falls within the range of the turbulence-generating motions. In order to take into account the presence of the peak in the turbulence energy spectrum that represents the direct input of energy at the discrete Strouhal frequency. Younis and Przulj [15] proposed that an additional term be included in the dissipation rate (Eq. 6) to enhance the rate of production of this quantity. This is most conveniently done by redefining the coefficient $C_{\varepsilon 1}$ thus

$$C^*_{\varepsilon 1} = C_{\varepsilon 1}\left(1 + C_t \frac{k}{\varepsilon}\frac{1}{Q+k}\left|\frac{\partial(Q+k)}{\partial t}\right|\right) \tag{8}$$

In the above, Q is the mean-flow kinetic energy per unit mass, and C_t is a coefficient whose value was determined in Ref. [15] by numerical optimization. Table 1 lists the values the turbulence model coefficients used. Extensive validation of this model modification using the experimental data from square and circular cylinders can be found in Ref. [15].

The modification to the $k-\varepsilon$ turbulent model given by Eq. (8) was implemented into the open-source software OPENFOAM. Details of the implementation can be found in Dai et al. [16].

In the present study, Eqs. (1)–(8) were discretized using finite-volume methodology, and solved iteratively using the pressure implicit with splitting of operator algorithm that couples the solution of the continuity and momentum equations to ensure that the predicted flow field satisfies both simultaneously.

2.2 Computational Model. The computations were performed for a two-dimensional cylinder having a square cross section of width $D = 6$ cm, and with corner radius $R = 0.96$ cm. In order to simplify the calculations and analysis, all dimensions are referenced to the cylinder width. The length of the computational domain was $36D$, and its width was $24D$. These dimensions were found by Younis and Przulj [15] to yield solutions that are not influenced by the boundary conditions or by blockage effects. The center of the square cylinder was located at $x = 12D$, and $y = 12D$ (Fig. 1). The blockage ratio B_f (defined as the ratio of cylinder width to domain width) was equal to 0.04167. For the cylinder with rounded corners, the ratio R/D was 0.16.

For the present computations, a structured hexahedral mesh was generated using the ICEM-CFD software which is interfaced with OPENFOAM. The outcome was a nonuniform grid distribution that very accurately captured the details of the rounded corners, while allowing for grid expansion in the far field in a manner consistent with accuracy and efficiency (Figs. 1(*a*) and 1(*b*). Since OPENFOAM is a three-dimensional flow solver, only one cell was placed in the spanwise direction in order to represent a two-dimensional computational field. This amounts to imposing a zero gradient boundary condition across the cell sides perpendicular to

Table 1 Turbulence model coefficients

Turbulence model	C_μ	σ_k	σ_ε	$C_{\varepsilon 1}$	$C_{\varepsilon 2}$	C_t
Standard $k-\varepsilon$	0.09	1.00	1.30	1.45	1.90	—
Modified $k-\varepsilon$	0.09	1.00	1.30	1.45	1.90	0.38

the spanwise direction. The normal distance (Δn_c /D) from the center of all cells in contact with the wall to the wall itself was 0.02. The nodes were concentrated near the cylinder wall with 40 cells being in contact with each side. For the rounded corner cylinder, the computational mesh that was found to yield grid-independent solutions (discussed later in the paper) consisted of 83,116 active cells, with the smallest grid size of cells bounded by the wall being 1.5 mm. The nondimensional time step ($\Delta t^* = ((U_0 \Delta t)/D)$) was set equal to 3.33×10^{-2} in order to capture the details of boundary layer flow. In order to monitor the time-variation of the wall static pressure, a total of 37 monitoring points were arranged around the cylinder's surface (Fig. 1(*c*)) with the pressure there, which was obtained by linear extrapolation from adjacent interior values, recorded at five time-step intervals. Computations were performed for two values of Reynolds number in the subcritical regime, namely, $\mathrm{Re} = 2 \times 10^4, 2 \times 10^5$.

The boundary conditions employed for both cases of sharp and rounded corners were as follows (see Fig. 1(*a*)). At the inlet, uniform profiles of the streamwise velocity (U), k, and ε were prescribed according to the specified Reynolds number. The value of k was based on the assumption of isotropic turbulence and an inlet level of relative turbulence intensity (u'/U) of 5%—a value which is typical for uniform turbulent streams. The dissipation rate was obtained from the definition of eddy viscosity (Eq. (4)) and by setting the ratio of eddy to molecular viscosity to 100. Tests were performed to determine the sensitivity of the computed results to the choice of inlet values. These tests showed that the effects were entirely negligible due to there being sufficient distance between

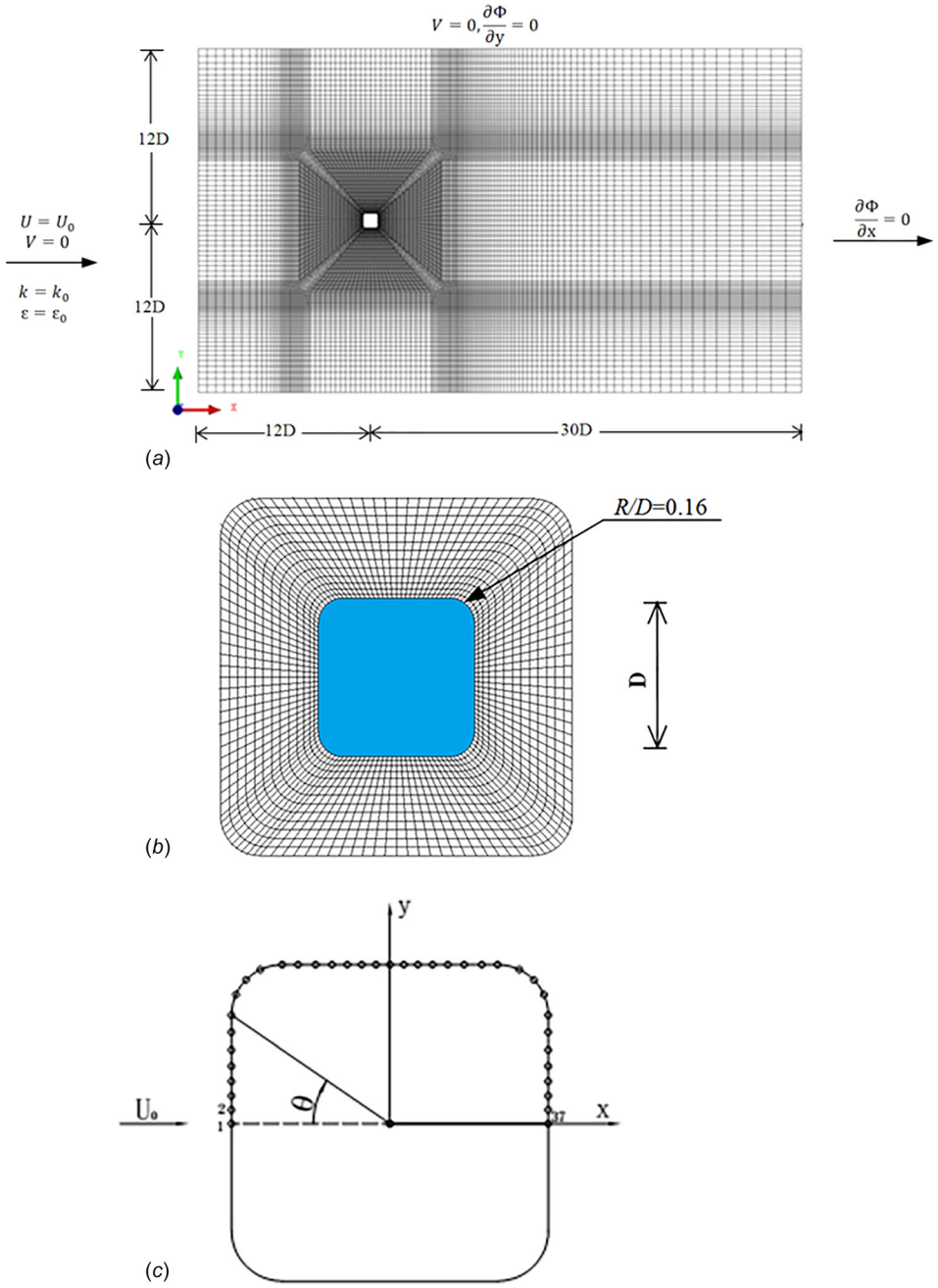

Fig. 1 Grid arrangement and boundary conditions: (*a*) grid distribution and computational domain, (*b*) mesh details near rounded corners, and (*c*) locations of pressure monitoring points

the inlet to the computational domain and the cylinder itself. At the outlet, the gradients of all dependent variables in the direction of flow were set equal to zero. The cylinder walls were assumed to be smooth, and the flow in their immediate vicinity was assumed to follow the universal logarithmic distribution

$$\frac{U}{u_\tau} = \frac{1}{\kappa}\ln\left(E\frac{\rho u_\tau \Delta y}{\mu}\right) \tag{9}$$

where ρ and μ are the density and dynamic viscosity, u_τ is the friction velocity, and Δy is the normal distance from the wall to the center of the grid nodes in contact with it. The coefficients E and κ were assigned their usual values of 9.0 and 0.41, respectively. The normal distance was adjusted to ensure that its value in wall coordinates (y^+) remained below 30. The boundary conditions for k and ε at the cylinder wall were fixed by the assumption of local equilibrium. Thus, the value of k at the nodes closest to the wall was fixed by reference to the wall shear stress (deduced from the friction velocity), and ε was set equal to the rate of production of k. The nondimensional time step for all the calculations Δt^* was chosen such that the value of Courant number was less than 1.0 everywhere in the computational domain, and at all times. The convergence criterion for the iterative process was set to be when the normalized absolute sum of the residuals of all variables fell to a value below 10^{-6}.

In discretizing equations (1)–(8), second-order accurate schemes were used for both temporal and spatial gradients. Specifically, the convection terms were discretized with the Gauss integral discrete lattice, the Laplacian term was discretized using the Gauss linear corrected scheme, while the time discretization scheme was implicit.

3 Results and Discussion

The need for the turbulence model modification presented in Eq. (8) in order to capture the occurrence in turbulent flows of vortex shedding at the appropriate strength is first demonstrated with reference to the flow around a square cylinder with sharp corners. Figure 2 presents the time histories of the lift and drag coefficients as predicted by the standard k–ϵ model (up until nondimensional time ($t* = 130$) followed by the results obtained after activation of the turbulence-model modification. It is clear that while the standard k–ϵ model does in fact capture the occurrence of vortex shedding, and it does so at a much reduced strength (in terms of root-mean-square of the oscillations in the force coefficients) compared to the modified model. There is a little doubt that the prediction of the effects of rounding the corners on the initiation and strength of vortex shedding will be in serious error if account is not taken of the interactions between the periodic mean-flow oscillations and the turbulence motions.

Prior to the presentation of the remaining results, we briefly present an assessment of the numerical accuracy of the simulations that will follow. This assessment was performed using the grid-convergence index (GCI) procedure as described in Eca et al. [17] and Celik et al. [18]. An estimate of the numerical discretization errors using this procedure is based on the Richardson extrapolation method. This entails the performing computations on three significantly different sets of nonuniform and structured grids having a total number of cells N1, N2, and N3 (N1 being the finest grid). In the present study, the ratio of the number of nodes in each successive refinement was around 1.20 (Table 2). The solutions obtained were then used to calculate the apparent order of accuracy of the method and the extrapolated values ϕ_{ext}^{21} which together yielded the value of the fine-grid convergence index (GCI_{fiine}^{21}). It can be seen from Table 2 that the numerical uncertainty in the fine-grid solution for the three variables examined (those being the average drag coefficient, and the root-mean-square values of both the lift and drag coefficients) amounts to under 8% of the theoretical GCI_{fiine}^{21} values and hence a mesh consisting of 83,116 active cells was adopted for all subsequent

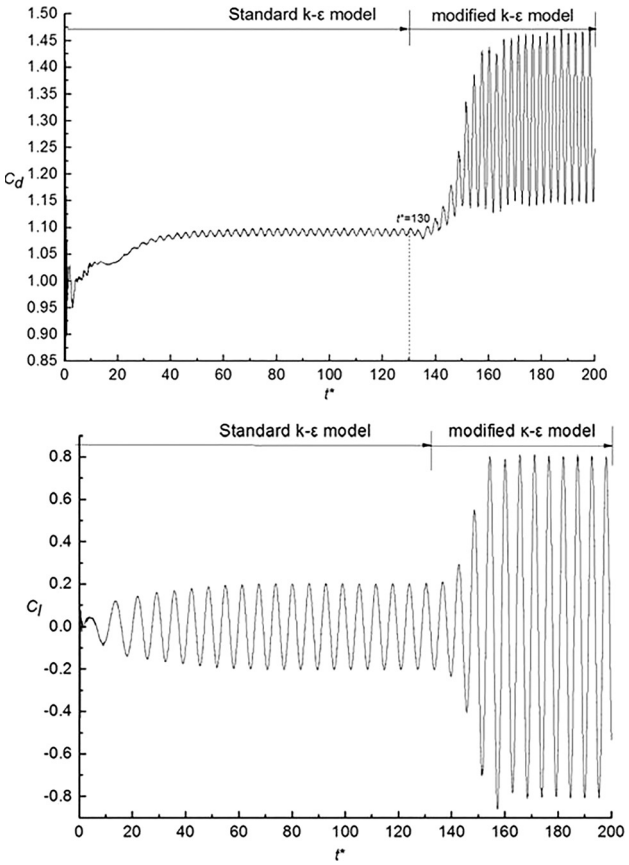

Fig. 2 Predicted variation of lift- and drag coefficients with time as obtained with the standard and the modified k–ϵ models for cylinder with rounded corners ($Re = 2.0\times10^4$)

calculations. Regarding assessment of the effect of time discretization on the numerical uncertainty, computations of flow around square with rounded corner were carried out with three different time-step sizes in order to quantify the extent of sensitivity to the choice of this parameter. All three time-step sizes chosen were consistent with the stability criterion that requires the Courant number to be less than 1.0 at every cell in the computational domain. Table 3 lists the nondimensional time-step sizes tested and the associated results. It can clearly be seen that the values of drag and lift coefficients show little dependence on the time-step size. This outcome demonstrates the extent to which convergence has been attained even with the largest time-step size. Thus, taking into consideration the requirements for computational

Table 2 The GCI method estimates of discretization error $\text{Re}=2.0\times10^5$

Variables/coefficients	$\Phi = C_d$	$\Phi = C_{\text{drms}}$	$\Phi = C_{\text{lrms}}$
N_1,N_2,N_3	103,760, 83,116, 68,824		
r_{21}	1.2484		
r_{32}	1.2077		
Φ_1	1.347	0.108	0.618
Φ_2	1.292	0.112	0.558
Φ_3	1.175	0.068	0.430
p	9.044	23.331	9.072
Φ_{ext}^{21}	1.379	0.108	0.653
e_a^{21}	0.041	0.044	0.097
e_{ext}^{21}	0.024	0.004	0.056
$\text{GCI}_{\text{fine}}^{21}$	0.029	0.0045	0.069

Table 3 Results for three time-step sizes obtained with the N_2 grid at Re=2.0×10^5

$\Delta t \times 10^{-4}$(s)	$\Delta t^* \times 10^{-3}$	C_d	C_{drms}	C_{irms}	St
0.5	3.330	1.2915	0.106	0.5575	0.202
2.5	16.700	1.2850	0.103	0.5560	0.200
5.0	33.300	1.2920	0.112	0.5580	0.192

accuracy and efficiency, the nondimensional time-step size was set equal to 3.33×10^{-2}.

In order to provide a baseline for assessing the effects of rounding the cylinder corners, we present first the results obtained for the subcritical flow around a sharp square cylinder. A further motivation for presenting these results is that this flow has already been extensively studied (e.g., Younis and Przulj [15]; Lyn et al. [19]; Yu and Kareem [20]; Rodi et al. [21]) and is hence suitable for validating the implementation of the turbulence-model modification into OPENFOAM. In what follows, the computational details were as given above, and the simulations were obtained for the case of Re $= 2 \times 10^4$.

Figures 3(*a*) and 3(*b*) show the predicted contours of the instantaneous velocity and pressure field around the square cylinder. It is apparent from these plots that a clearly defined vortex shedding process is captured by the calculations. Figure 4 presents the corresponding time histories of the drag and lift coefficients, while a detailed comparison between the predicted and experimentally measured nondimensional parameters that characterize this flow is shown in Table 4. It is clear from this table that the numerical results from the modified turbulence model are in good accord with the measurements [4,8,15,19,21,22] and are in line with the results obtained using the more computationally intensive large eddy simulations [23]. These results serve to demonstrate the capabilities of the computational method and the modified turbulence closure for the case of sharp corners. In what follows, we turn to the key problem addressed here, namely, that of the flow around a square cylinder with rounded corners.

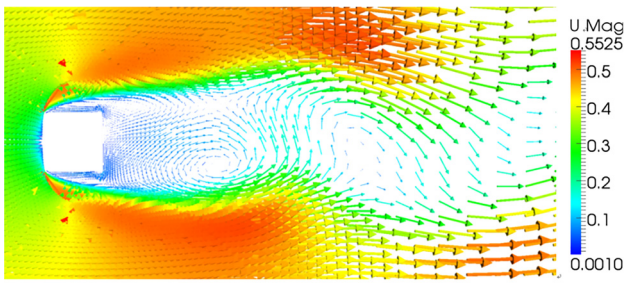

(*a*)

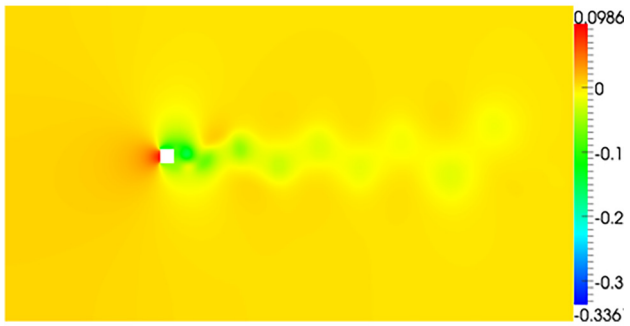

(*b*)

Fig. 3 Contours of velocity and pressure for square cylinder with sharp corners (Re = 2.0×10^4): (*a*) velocity contours and (*b*) pressure contours

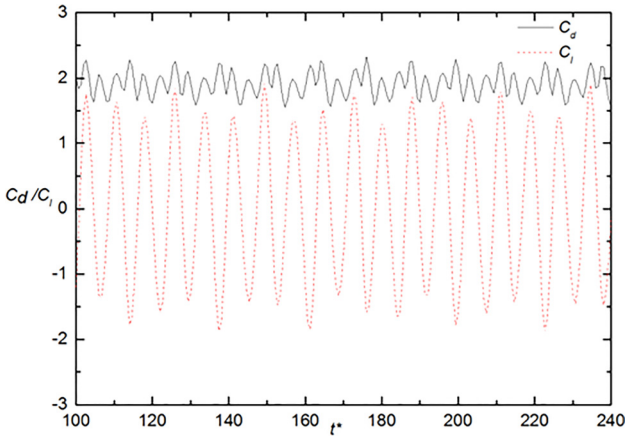

Fig. 4 Time history of C_d and C_l of square cylinder with sharp corners (Re = 2.0×10^4)

The computational geometry and boundary conditions for the cylinder with rounded corners are identical to those of the previous case and differences in the computed results are therefore entirely due to the geometry effects. We consider two Reynolds numbers in subcritical regime to study the effect of rounded corner on the flow features and hydrodynamic parameters. In order to analyze the pressure distribution along the cylinder walls, monitoring points were set on the cylinder wall at 5 deg intervals.

Figure 5 presents close-up views of the predicted instantaneous velocity vectors and streamlines for both sharp- and round-cornered cylinders. The effects of rounding the corners are most evident in the much reduced size of the separated flow zone along the top surface and consequently in the smaller vortex generated downstream of the rounded cylinder.

We turn to consideration of the long-time-averaged wall static pressure distributions. Since the geometry and inlet conditions are symmetric around the midplane, it follows that the computed $Cp - \theta$ curves for the upper and lower halves of the cylinder were identical, and hence, these are presented for the top half only. Figures 6(*a*) and 6(*b*) show the predicted circumferential variation of wall static pressure for the two Reynolds numbers considered. Also, shown there are the results obtained for the sharp-cornered cylinder as well as some representative measurements [22,24]. The effects of rounding the cylinder corners are expected to delay flow separation and hence produce a narrower separated wake. This is evident in the present predictions at both Reynolds numbers, most clearly in the greater pressure recovery on the leeward face, leading, as will be discussed later, to lower drag compared to the sharp-cornered geometry. The agreement with the experimental data is not particularly close but it should be noted that the experiments themselves show a similar degree of variation. Figure 6 also shows that the minimum pressure is attained at the front

Table 4 Computed and measured bulk parameters for square cylinder (Re=2.0×10^4)

	$\overline{C}_d$	C_{drms}	C_{irms}	St
Present work	2.00	0.204	1.13	0.130
Tamura and Miyagi [4] (Re = 3 × 10^4)	2.10	—	1.05	0.130
Carassale et al. [8] (Re = 3.7 × 10^4)	2.06	—	1.02	0.125
Younis and Przulj [15]	2.16–2.28	0.18–0.23	1.10–1.40	0.13–0.139
Lyn et al. [19]	2.05	—	—	0.132
Yu and Kareem [20]	2.14	0.250	1.15	0.135
Rodi et al. [21]	2.30	0.140	1.15	0.130
Lee [22]	2.05	0.220	1.22	0.130
Sohankar et al. [23]	2.03	0.200	1.23	0.126

corner irrespective of whether the cylinder corners were sharp or rounded. For the case of the rounded corner, there is an increase in the values of the time-averaged wall static pressure at the base region of the cylinder, especially when θ is between 90 deg and 180 deg. With Reynolds number increasing from 2×10^4 to 2×10^5, the presence of rounded corners causes the point of minimum value to be located at a value of θ value of around 50 deg, while rounded corners have little effect on the separation point at the front corners at subcritical Reynolds number. The minimum Cp for cylinder with and without rounded corners obviously reduces from around -1.7 to -2.1 and -1.55 to -1.59 due to increasing Re.

The variation of root-mean-square of the fluctuating pressure coefficients with θ is shown in Fig. 7. It is clearly evident that rounded corner cylinder decreases the peak of Cp' value in the interval 45 deg $\leq \theta \leq$ 180 deg. For $\mathrm{Re} = 2 \times 10^5$, the peaks of Cp' value for the rounded cylinder appear in the vicinity of 50 deg and 145 deg, respectively, which is due to the second separation of the flow at rounded corner of downstream. While for the sharp square cylinder, the main peak of Cp' value appears about 45 deg, and is much larger than for the rounded cylinder. For this geometry, the second smaller peak appears at 135 deg. With increasing Re from 2×10^4 to 2×10^5, the maximum Cp' value is clearly increasing form about 0.68 to 0.72 for rounded corner cylinder. All these changes clearly indicate that the second separation of boundary layer at back corners is delayed due to the influence of the rear rounded corner.

Turning to the total forces on the cylinder, Fig. 8 shows the time history of the nondimensional drag and lift for the rounded cylinder within the overall time of simulations. In the beginning, and under the influence of the assumed uniform initial conditions, nonperiodic oscillations are present that eventually give way to the establishment of a fully periodic behavior. The modified turbulence model was used throughout these simulations and these results demonstrate its ability to capture both the initiation and subsequent development of the vortex shedding field.

Figures 9 and 10 show the effects of rounding the cylinder corners on the time history of the force coefficients. It can be seen that rounding the corners causes the time-averaged and root-mean-square values of both the drag and lift forces to markedly decrease, for the same Reynolds number. The influence of the rounded corners on the mean and the fluctuating force coefficients ($\overline{C}_d$, C_{drms}, and C_{lrms}) can clearly be seen in Tables 5 and 6. For the case of the cylinder with sharp corners, the predicted $\overline{C}_d$ value of 2.0 at $\mathrm{Re} = 2 \times 10^4$, which is in close agreement with the measurements of Tamura and Miyagi [4] and Carassale et al. [8], is seen to drop by 30% as a result of rounding the corners. For the

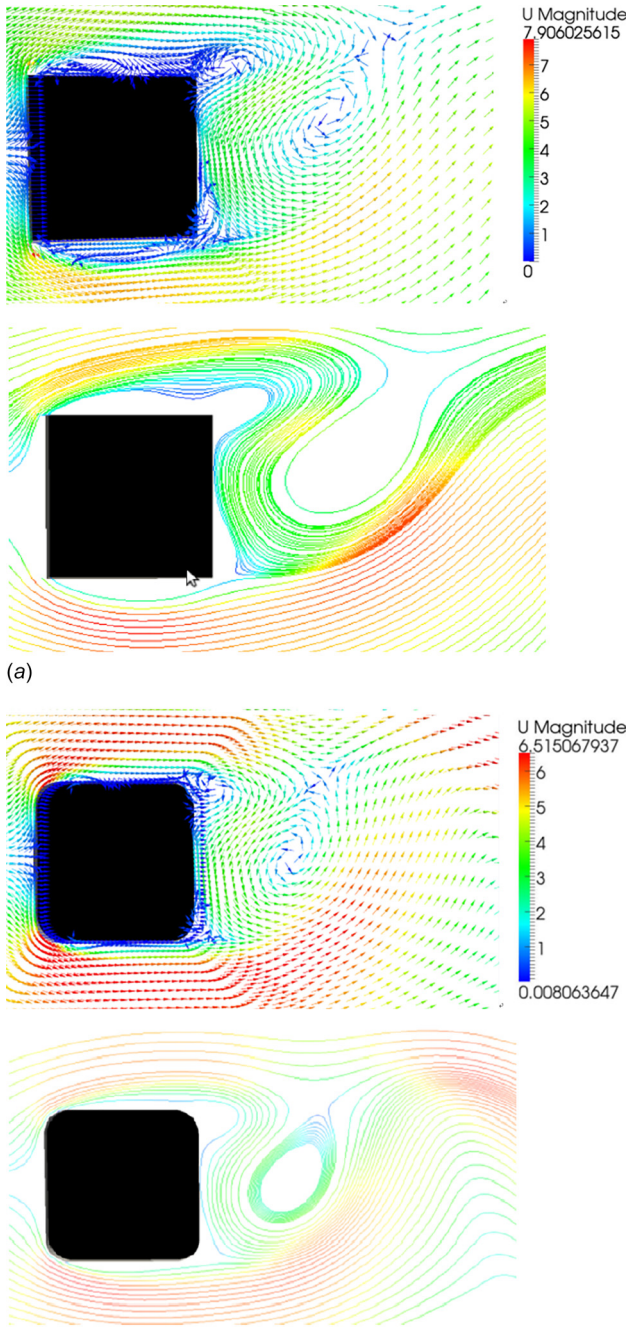

Fig. 5 Instantaneous velocity vectors and streamlines of square cylinder at Re = 2.0×10⁴: (*a*) sharp-cornered cylinder and (*b*) rounded corners cylinder

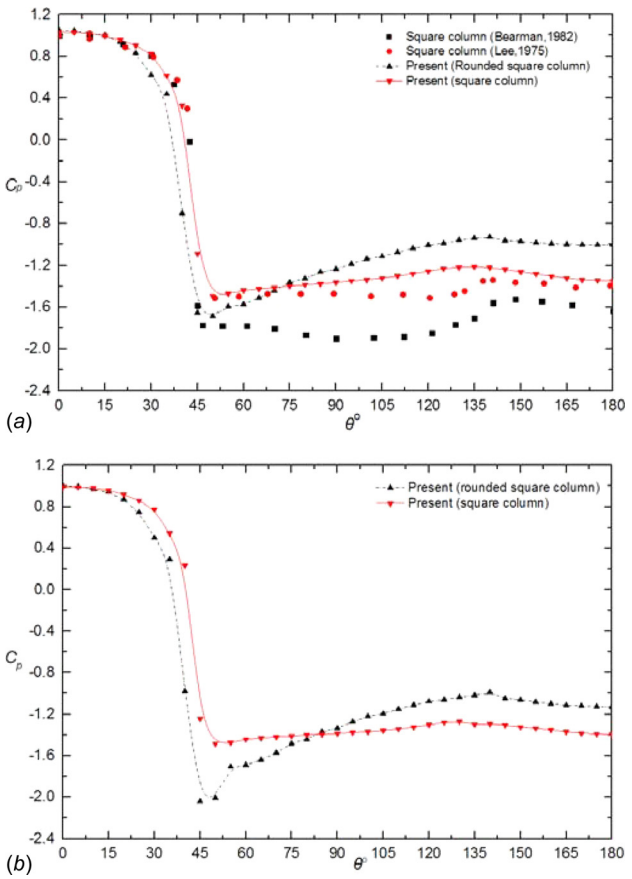

Fig. 6 Predicted and measured mean wall static pressure distribution: (*a*) Re = 2.0×10⁴ and (*b*) Re = 2.0×10⁵

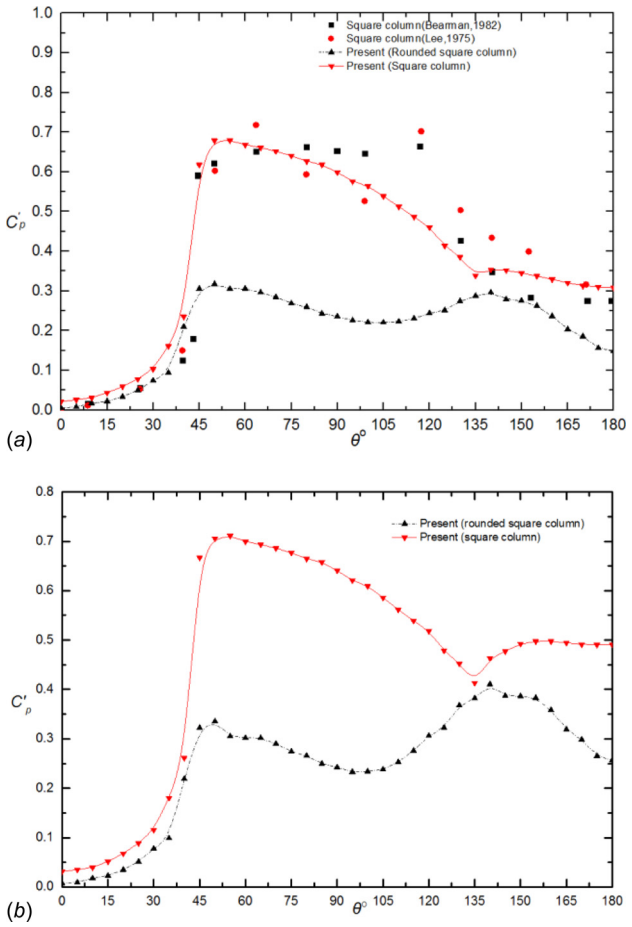

Fig. 7 Predicted variation of fluctuating pressure versus θ: (*a*) Re = 2.0×10^4 and (*b*) Re = 2.0×10^5

rounder corner cylinder, the computed $\overline{C}_d$, C_{drms}, and C_{lrms} values are 1.34, 1.13, and 0.51, respectively. The same coefficients are obtained in the measurements of Tamura and Miyagi [4] for the same ratio of corner radius to cylinder width and at Re = 3.0×10^4 as 1.22, 1.08, and 0.40. Carassale et al. [8] experiments were conducted on a cylinder with rounded corner ratio of 0.133 and at Re = 2.7×10^4. Their reported values for the same coefficients were 1.42, 1.02, and 0.50, respectively. The agreement between the present predictions and the results from two different experiments is clearly quite good. For the higher Reynolds number of Re = 2×10^5, the computed value of $\overline{C}_d$ value reduces from a value of 1.932 for the square cylinder to 1.292 for the rounded corners case. These values correspond closely with the experimental results of Delany and Sorensen [12] at the same Reynolds number and rounded corner ratio where the $\overline{C}_d$ value dropped from 2.0 to 1.2. It can be seen from Table 5 that the effect of rounded corners on C_{drms} value causes it to decrease by over 60%, while C_{lrms} decreases by about 55%.

As before, the Strouhal frequency of the vortex shedding is obtained by performing fast Fourier transform on the time series of the fluctuating lift coefficients. This is shown in Fig. 11 where it is evident that the effects of the rounded corners are to greatly reduce the energy content of the shed vortices, while increasing the magnitude of the dominant frequency to a value that yields a Strouhal number (Table 6) that is very close to that found for circular cylinders at similar Reynolds number [12].

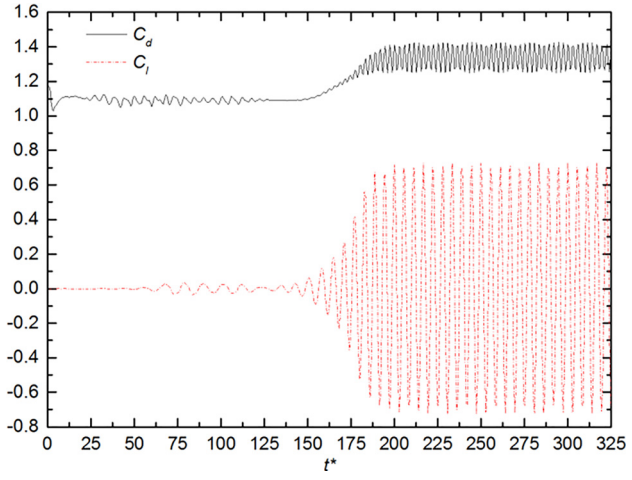

Fig. 8 Time history of drag and lift coefficients for rounded corners cylinder (Re = 2×10^4)

4 Conclusions

This work is concerned with predicting the influence of rounded corners on the hydrodynamic loads on a square cylinder in a steady turbulent current. The simulations were performed using a modified k–ϵ turbulence model which was implemented into the open source OPENFOAM simulations software. The benchmark flow past a square cylinder with sharp corners was first computed to validate the implementation. The results obtained were in good accord with the measured data and with other computations. Thereafter, the flow past a square cylinder with rounded corners was simulated at two values of Reynolds number in the subcritical

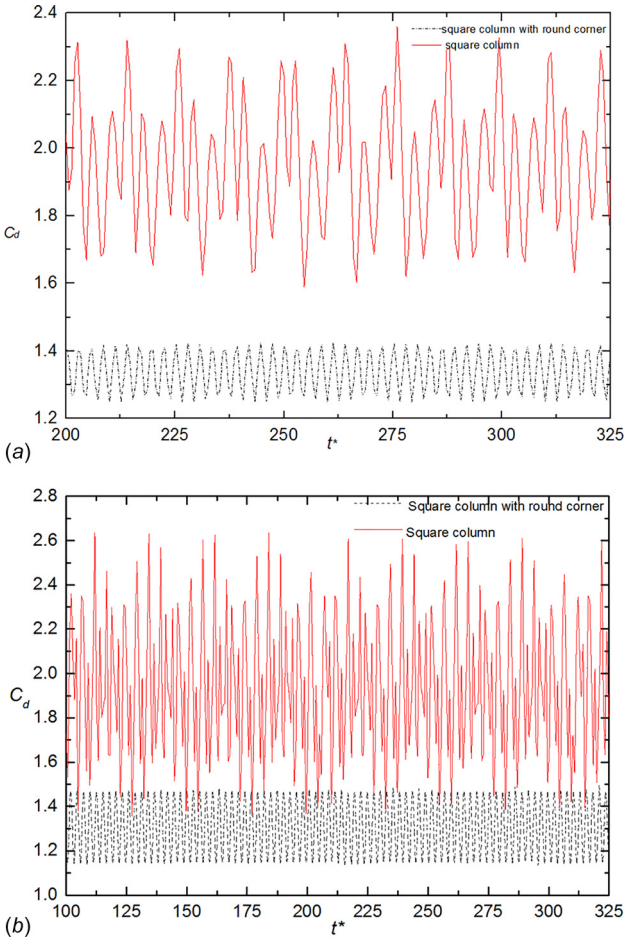

Fig. 9 Comparison of time history of drag for square column with rounded corners at different Reynolds number: (*a*) Re = 2.0×10^4 and (*b*) Re = 2.0×10^5

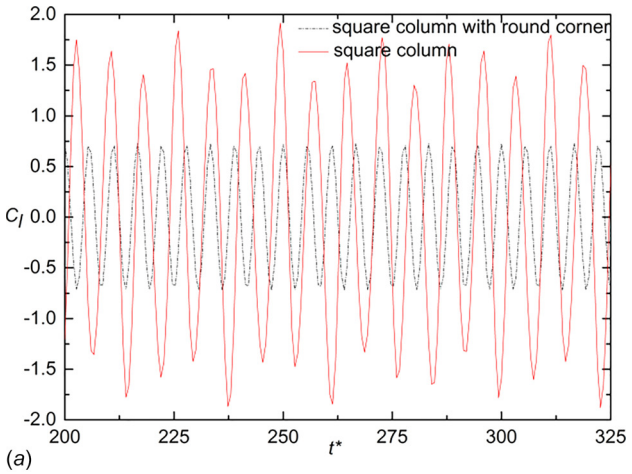

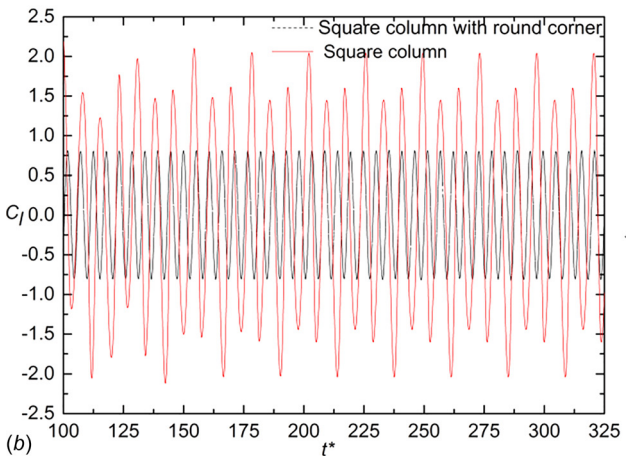

Fig. 10 Comparison of time history of lift forces for square column with rounded corners at different Reynolds number: (*a*) Re = 2.0×10^4 and (*b*) Re = 2.0×10^5

regime. Comparisons of the hydrodynamic coefficients with the sharp-cornered values showed that the effects of rounded corners are to progressively decrease both the mean and fluctuating drag coefficients relative to the sharp-corner values. It was noted that the decrease in the fluctuating lift coefficient was somewhat less than for the fluctuating drag. Plots of the predicted streamlines

Table 5 Comparison of mean and root-mean-square drag coefficients for square cylinder with and without rounded corners at different Re

	$\overline{C_d}$			C_{drms}		
Re	Square	Rounded corners	% change	Square	Rounded corners	% change
2×10^4	2.000	1.340	−33.00	0.204	0.074	−63.72
2×10^5	1.932	1.292	−33.13	0.325	0.110	−66.15

Table 6 Predicted root-mean-square lift coefficients and St for square cylinder with and without rounded corners at different Re

	C_{lrms}			St		
Re	Square	Rounded corners	% Change	Square	Rounded corners	% Change
2×10^4	1.13	0.51	−54.86	0.13	0.187	+43.85
2×10^5	1.22	0.558	−54.26	0.126	0.192	+52.38

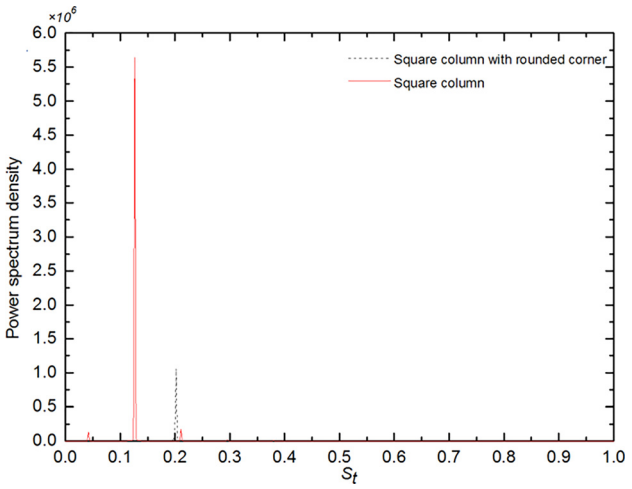

Fig. 11 Predicted power spectrum of fluctuating lift coefficients for square column with and without rounded corners at Re = 2.0×10^5

show that the leeward rounded corners have the effect of causing the flow separation angle to move further downstream thereby increasing the base pressure. Inspection of the power spectrum of the fluctuating lift forces confirm that the delayed separation due to rounded corners drastically reduces the strength of the vortex shedding and increases the Strouhal number to a value close to that of a round cylinder. Overall, the present result suggest that the effects of vortex shedding due to a square cylinder with rounded corners can be predicted to acceptable engineering accuracy using URANS methodology provided that the interactions between the periodic mean-flow motions and the random turbulence are properly accounted for in the turbulence closure.

Acknowledgment

We gratefully acknowledge the support provided by the National Natural Science Foundation of China (Grant No. 11472087).

Nomenclature

A = projected area
B_f = blockage ratio
D = cylinder width
C_d = drag coefficient ($= \overline{F_d}/0.5\rho U_\infty^2 A$)
C_{drms} = fluctuating drag coefficient ($= \sqrt{(\sum [F_d(t) - \overline{F_d}(t)]^2/N)}/0.5\rho U_\infty^2 A$)
C_{lrms} = fluctuating lift force coefficient ($= \sqrt{(\sum [F_l(t) - \overline{F_l}(t)]^2/N)}/0.5\rho U_\infty^2 A$)
f_s = frequency of vortex shedding
k = turbulence kinetic energy
P_k = production rate of the turbulence kinetic energy
Q = mean-flow kinetic energy ($= \frac{1}{2} U_i U_i$)
R = radius of rounded corner
Re = Reynolds number ($= UD/\nu$)
St = Strouhal number ($= f_s D/U_\infty$)
u_i = fluctuating velocity components
u_τ = friction velocity
U_i = mean velocity components
U_∞ = velocity of incident flow
$\overline{u_i u_j}$ = Reynolds-stress tensor

Greek Symbols

δ_{ij} = Kronecker delta
Δt^* = nondimensional time-step ($= \Delta t \cdot U_0/D$)

Δn_c = normal distance from the cell center to the wall
ε = turbulence energy dissipation rate
κ = von Karman constant
μ = dynamic viscosity
υ = kinematic viscosity
υ_t = eddy viscosity
ρ = fluid density
θ = circumferential angle

Subscript

i, j = Cartesian tensor indices

References

[1] Bearman, P. W., Graham, J. M. R., Obasaju, E. D., and Drossopoulos, G. M., 1984, "The Influence of Corner Radius on the Force Experienced by Cylindrical Bluff Bodies in Oscillatory Flow," Appl. Ocean Res., **6**(2), pp. 83–89.
[2] Kawai, H., 1998, "Effect of Corner Modifications on Aeroelastic Instabilities of Tall Buildings," J. Wind Eng. Ind. Aerodyn., **74–76**(1), pp. 719–729.
[3] Tamura, T., Miyagi, T., and Kitagishi, T., 1998, "Numerical Prediction of Unsteady Pressures on a Square Cylinder With Various Corner Shapes," J. Wind Eng. Ind. Aerodyn., **74–76**, pp. 531–542.
[4] Tamura, T., and Miyagi, T., 1999, "The Effect of Turbulence on Aerodynamic Forces on a Square Cylinder With Various Corner Shapes," J. Wind Eng. Ind. Aerodyn., **83**(1–3), pp. 135–145.
[5] Dalton, C., and Zheng, W., 2003, "Numerical Solutions of a Viscous Uniform Approach Flow Past Square and Diamond Cylinders," J. Fluids Struct., **18**(3–4), pp. 455–465.
[6] Miran, S., and Sohn, C. H., 2015, "Numerical Study of the Rounded Corners Effect on Flow Past a Square Cylinder," Int. J. Numer. Methods Heat Fluid Flow, **25**(4), pp. 686–702.
[7] Jaiman, R. K., Sen, S., and Gurugubelli, P. S., 2015, "A Fully Implicit Combined Field Scheme for Freely Vibrating Square Cylinders With Sharp and Rounded Corners," Comput. Fluids, **112**, pp. 1–18.
[8] Carassale, L., Freda, A., and Marre-Brunenghi, M., 2014, "Experimental Investigation on the Aerodynamic Behavior of Square Cylinders With Rounded Corners," J. Fluids Struct., **44**, pp. 195–204.
[9] Ajith Kumar, R., Sohn, C. H., and Lakshmana Gowda, B. H., 2009, "Influence of Corner Radius on the Near Wake Structure of a Transversely Oscillating Square Column," J. Mech. Sci. Technol., **23**(9), pp. 2390–2416.
[10] Hu, J. C., Zhou, Y., and Dalton, C., 2005, "Effects of the Corner Radius on the Near Wake of a Square Prism," Exp. Fluids, **40**(1), pp. 106–118.
[11] Nidhul, K., 2014, "Influence of Corner Geometry on the Flow Structure and Flow Characteristics for Flow Past a Square Column at Re=150," Int. J. Res. Aeronaut. Mech. Eng., **2**, pp. 32–41.
[12] Delany, N. K., and Sorensen, N. E., 1953, "Low Speed Drag of Cylinders of Various Shapes," National Advisory Committee for Aeronautics, Washington, DC, Technical Note NACA-3038.
[13] Murakami, S., 1993, "Comparison of Various Turbulence Models Applied to a Bluff Body," J. Wind Eng. Ind. Aerodyn., **46–47**, pp. 21–36.
[14] Tsuchiya, M., Murakami, S., Mochida, A., Kondo, K., and Ishida, Y., 1997, "Development of a New Model for Flow and Pressure Fields Around Bluff Body," J. Wind Eng. Ind. Aerodyn., **67–68**, pp. 169–182.
[15] Younis, B. A., and Przulj, V. P., 2006, "Computation of Turbulent Vortex Shedding," Comput. Mech., **37**(5), pp. 408–425.
[16] Dai, S. S., Younis, B. A., and Sun, L. P., 2015, "OpenFOAM Predictions of Hydrodynamics Loads on Full-Scale TLP," Ocean Eng., **102**(1), pp. 162–173.
[17] Eca, L., Hoekstra, M., and Roache, P. J., 2007, "Verification of Calculations an Overview of the 2nd Lisbon Workshop on CFD Uncertainty Analysis," AIAA Paper No. 2007–4089.
[18] Celik, I. B., Ghia, U., Roache, P. J., Freitas, C. J., Coleman, H., and Read, P. E., 2008, "Procedure for Estimation and Reporting of Uncertainty Due to Discretization in CFD Applications," ASME J. Fluids Eng., **130**(7), p. 078001.
[19] Lyn, D. A., Einav, S., Rodi, W., and Park, J. H., 1995, "A Laser Doppler Velocimetry Study of Ensemble-Averaged Characteristics of the Turbulent Near Wake of a Square Cylinder," J. Fluid Mech., **304**, pp. 285–319.
[20] Yu, D. H., and Kareem, A., 1997, "Numerical Simulation of Flow Around Rectangular Prism," J. Wind Eng. Ind. Aerodyn., **67–68**, pp. 195–208.
[21] Rodi, W., Ferziger, J. H., Breuer, M., and Pourquie, M., 1997, "Status of Large Eddy Simulation: Results of a Workshop," ASME J. Fluids Eng., **119**(2), pp. 248–262.
[22] Lee, B. E., 1975, "The Effect of Turbulence on the Surface Pressure Field of a Square Prism," J. Fluid Mech., **69**(2), pp. 263–282.
[23] Sohankar, A., Davidson, L., and Norberg, C., 2000, "Large Eddy Simulation of Flow Past a Square Cylinder: Comparison of Different Subgrid Scale Models," ASME J. Fluids Eng., **122**(1), pp. 39–47.
[24] Bearman, P. W., and Obasaju, E. D., 1982, "An Experimental Study of Pressure Fluctuations on Fixed and Oscillating Square-Section Columns," J. Fluid Mech., **119**, pp. 297–321.